

Chemical Science

Accepted Manuscript

This article can be cited before page numbers have been issued, to do this please use: F. Gilch, J. Brossette, F. F. Westermair, W. Silva, G. Balázs, R. M. Gschwind, H. Zipse and R. Wolf, *Chem. Sci.*, 2026, DOI: 10.1039/D6SC01229A.



This is an Accepted Manuscript, which has been through the Royal Society of Chemistry peer review process and has been accepted for publication.

Accepted Manuscripts are published online shortly after acceptance, before technical editing, formatting and proof reading. Using this free service, authors can make their results available to the community, in citable form, before we publish the edited article. We will replace this Accepted Manuscript with the edited and formatted Advance Article as soon as it is available.

You can find more information about Accepted Manuscripts in the [Information for Authors](#).

Please note that technical editing may introduce minor changes to the text and/or graphics, which may alter content. The journal's standard [Terms & Conditions](#) and the [Ethical guidelines](#) still apply. In no event shall the Royal Society of Chemistry be held responsible for any errors or omissions in this Accepted Manuscript or any consequences arising from the use of any information it contains.

ARTICLE

Selective White Phosphorus Activation and Functionalization with Inorganic Grignard Reagents

Franziska Gilch,^a Jan Brossette,^b Franz Westermair,^c Wagner Menezes da Silva,^c Gábor Balázs^a, Ruth Gschwind,^{*c} Hendrik Zipse,^{*b} and Robert Wolf^{*a}

Received 00th January 20xx,
Accepted 00th January 20xx

DOI: 10.1039/x0xx00000x

We describe the targeted and selective functionalization of white phosphorus (P_4) using 'inorganic Grignard reagents'. Reactions of the Fe-Mg complexes $[(DippBDI)Mg(THF)_x Fp]$ ($Fp = CpFe(CO)_2$, **1**: $x = 0$; **1-THF**: $x = 1$, $DippBDI = 2,6$ -diisopropylphenyl-1,3-diketiminato) and $[(DippBDI)MgFp^*]$ (**2**, $Fp^* = Cp^*Fe(CO)_2$) afford the compounds $[(DippBDI)Mg(THF)_x][Fp(\mu-P_4)]$ (**3**: $x = 0$; **3-THF**: $x = 1$) and $[(DippBDI)Mg][Fp^*(\mu-P_4)]$ (**4**) featuring P_4^{2-} ligands with a 'butterfly' structure bridging Fe and Mg. The coordination of the β -diketiminato magnesium cations $[(DippBDI)Mg]^+$ plays a key role in stabilizing these reactive ' P_4 -butterfly' anions through non-covalent Mg–P bonds and dispersion forces. Thermolysis or photolysis of **3-THF** and **4** afforded rare tetraphosphacyclopentadienolate complexes **7** and **8**. Complex **4** exhibits unmitigated reactivity towards a wide range of main group element electrophiles (iPrNCNiPr, Ph_2BCl , Ph_3SnCl (Me_3Si) $_3SiCl$ and Me_2PCl), furnishing rare examples of stable, mixed-substituted tetraphosphanes **9-13** as well as an octaphosphane **14** featuring a Sn_2P_8 core.

Introduction

White phosphorus (P_4) is the only molecular allotrope of phosphorus stable at room temperature and serves as a crucial feedstock for phosphorus-based chemicals.^[1] Because of its important role in the phosphorus industry and its multifaceted and often poorly predictable reactivity, the chemistry of P_4 is a subject of significant current interest. Although many procedures for P_4 activation using main-group elements and transition metals have been reported, the targeted, selective functionalization of the resulting polyphosphorus frameworks lags behind simple P_4 activation.^[2]

The bicyclo[1.1.0]tetraphosphabutane motive (' P_4 -butterfly') resulting from the cleavage of one P–P bond of the P_4 tetrahedron represents the first step in P_4 activation.^[3,4,16-25] The synthesis of ' P_4 -butterfly' compounds has been achieved by reaction of P_4 with main-group radicals and transition-metal-based radicals,^[3] as well as using carbenes and heavier carbene analogues.^[4] Reactions of this type result in the generation of symmetrical P_4 -butterfly species of types **A** or **B** (Figure 1). Due to the strong, covalent phosphorus-element bonds, these species typically exhibit attenuated reactivity and limited potential for further functionalization. In contrast, the reaction of P_4 with charged nucleophiles affords highly reactive anions $[RP_4]^-$ (**C**), which tend to decompose quickly.^[5,6] Nonetheless, alkali metal salts of type $M[HP_4]$ have been characterised by ^{31}P NMR spectroscopy at low temperature.^[5,7] Lammertsma and coworkers have reported that $[RP_4]^-$ anions (**C**) containing

sterically demanding aryl groups or the Fp^* - anion ($Fp^* = Cp^*Fe(CO)_2$, $Cp^* = C_5Me_5$) can be stabilized by the coordination of boranes such as BPh_3 and $B(C_6F_5)_3$ to one of the wingtip phosphorus atoms (**D**, Figure 1a, $R =$ bulky aryl or Fp^*).^[8-12] However, the reactivity of these species has been limited to protonation and alkylation reactions, a [3+1] fragmentation reaction induced by $PhNCO$ and Lewis acid coordination with BH_3 , BPh_3 , $W(CO)_5$ and $[Au(IPr)]^+$ [$IPr = 1,3$ -bis(2,6-diisopropylphenyl)imidazolin-2-ylidene]. The P_4 -butterfly species **E** resulting from the functionalization of **D** with $R'X$ decomposes with $R' = H$ or Me , but can be isolated when the sterically demanding alkyl groups such as Ph_3C are employed.^[8,11,12]

Recently, we have shown that the combination of a redox-active 3d-metal cation with a main-group element, such as Ga, Si, Sn, or a redox non-innocent d-block element such as Zn, facilitates P_4 activation.^[13] In contrast, the use of transition-metal-magnesium complexes ('inorganic Grignard reagents') for P_4 activation has hardly been explored,^[14,15,16] despite recent studies demonstrating the significant potential of low-valent magnesium and calcium complexes for P_4 storage and activation (Figure 1, complexes **F-H**, Figure 1).^[17,18] Here, we demonstrate that the inorganic Grignard reagents $[(DippBDI)MgFp(THF)_x]$ (**1**: $x = 0$; **1-THF**: $x = 1$, $Fp = CpFe(CO)_2$, $DippBDI = 2,6$ -diisopropylphenyl-1,3-diketiminato) and $[(DippBDI)MgFp^*]$ (**2**) selectively afford P_4 -butterfly complexes $[(DippBDI)Mg(THF)_x Fp(\mu-P_4)]$ (**3**: $x = 0$; **3-THF**: $x = 1$) and $[(DippBDI)MgFp^*(\mu-P_4)]$ (**4**). The reversible nature and the mechanism of the P_4 activation reaction are investigated using variable-temperature ^{31}P NMR spectroscopy, 1H exchange NMR spectroscopy, and DFT calculations. An analysis of the non-covalent interactions highlights the essential role of the magnesium cation in stabilizing the complexes. Thermolysis or photolysis of **3-THF** and **4** generate rare tetraphosphacyclopentadienolate transition metal complexes **7**

^a Universität Regensburg, Institut für Anorganische Chemie, 93040 Regensburg, Germany. E-Mail: robert.wolf@ur.de

^b Ludwig-Maximilians-Universität München, Institut für Chemie, Butenandtstr. 5-13, 81377 München, Germany. E-mail: zipse@cup.uni-muenchen.de

^c Universität Regensburg, Institut für Organische Chemie, 93040 Regensburg, Germany. E-Mail: ruth.gschwind@ur.de

† Footnotes relating to the title and/or authors should appear here.

Supplementary Information available: [details of any supplementary information available should be included here]. See DOI: 10.1039/x0xx00000x



and **8**. Additionally, we show that 'P₄-butterfly' ligand in **4** is readily functionalized with various electrophiles. These reactions afford unprecedented mixed-substituted bicyclo[1.1.0]tetraphosphabutanes of type Fp*P₄R [**9-13**, R = C(NⁱPr)₂ (**9**), BPh₂ (**10**), SnPh₃ (**11**), Si(SiMe₃)₃ (**12**), PMeS₂ (**13**)] as well as the octaphosphane [Ar₂Sn₂P₈Fp*₂] (**14**, Ar = 2,6-(2,6-ⁱPr₂-C₆H₃)-C₆H₃). Our results demonstrate that inorganic Grignard reagents act as effective metal-based Lewis pairs, enabling the selective activation of P₄ and the targeted functionalization of the resulting P₄²⁻ ligand.

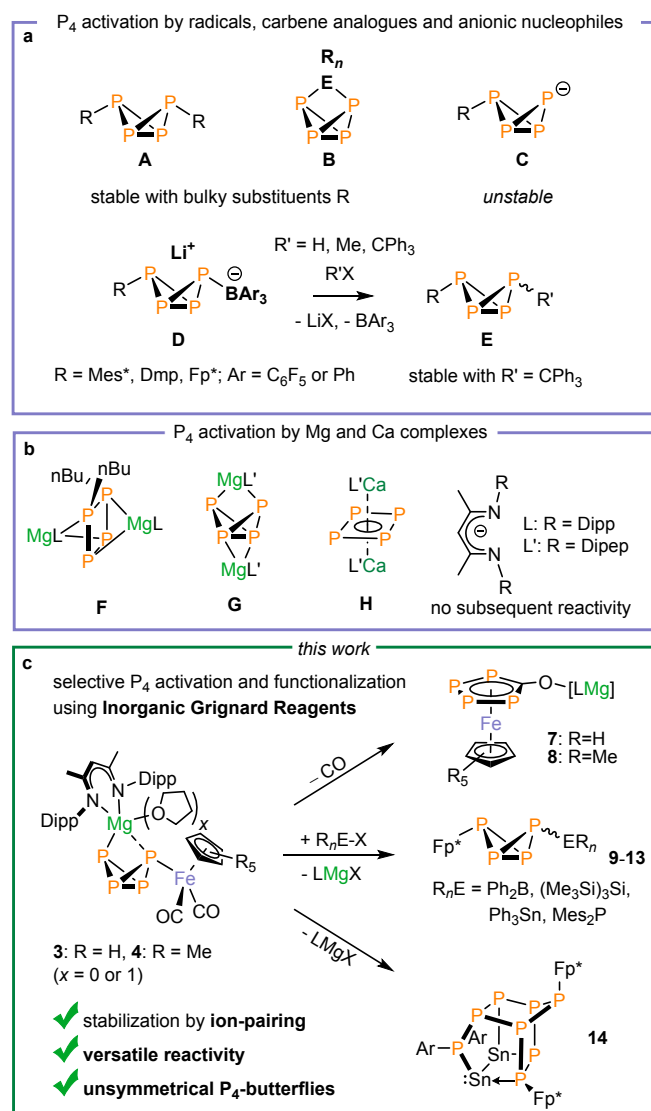


Figure 1. a) Bicyclo[1.1.0]tetraphosphabutanes and related anions **A-E** resulting from the reaction of P₄ with radicals, carbene analogues, and nucleophilic anions. (b) Reaction products of P₄ with BDI-stabilized Mg(II), Mg(I) and Ca(I) complexes. (c) Selective P₄ activation and functionalization enabled by Mg-Fe pairs (this work; Mes* = 2,4,6-tBu₃C₆H₂, Dmp = 2,6-Me₂-C₆H₃, Dipp = 2,6-diisopropylphenyl, Dipep = 2,6-diisopentylphenyl, Ar = 2,6-(2,6-ⁱPr₂-C₆H₃)-C₆H₃).

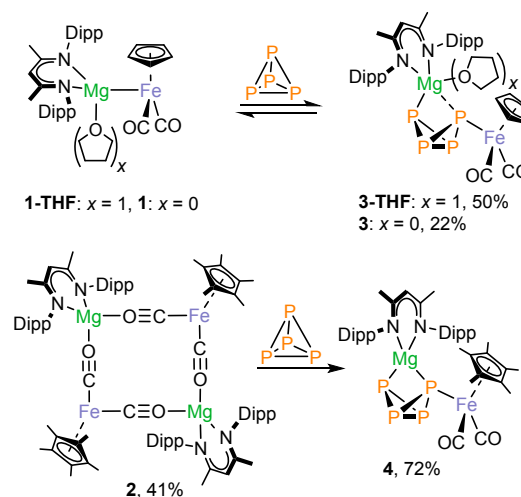
Results and Discussion

View Article Online

DOI: 10.1039/D6SC01229A

Synthesis and characterization of P₄-butterfly complexes

Inspired by the work of Crimmin and Mountford on the use of the inorganic Grignard reagents **1** and **1-THF** in C–F activation and heterocumulene insertion,^[14,15] we investigated their reactivity with P₄. Initial ³¹P NMR spectroscopic studies showed that P₄ readily inserts into the Mg–Fe bond of **1-THF** in THF-d₈ or C₆D₆ to generate **3-THF**, which gives rise to an AMX₂ spin system. Likewise, the reaction of **1** with P₄ in toluene-d₈ afforded the THF-free analog **3**. Complexes **3** and **3-THF** can be isolated as air-sensitive yellow-orange crystals in moderate yields (50% and 22%, respectively). The AMX₂ spin systems observed in the ³¹P NMR indicate the formation of a P₄-butterfly structure. The ²J_{PP} coupling constants between the wingtip P atoms (47.0 and 36.8 Hz) indicate an *endo,exo* configuration of the butterfly-P₄ ligands,^[10,12,19] suggesting that there is no through-space interaction between these P atoms.^[20] The ¹H and ³¹P NMR spectra furthermore indicate that **3** and **3-THF** are in an equilibrium with the starting materials **1** and **1-THF** and P₄ in deuterated benzene and deuterated THF (vide infra).



Scheme 1. Synthesis of complexes **3-THF**, **3** and **4**. The reaction is reversible with **3** and **3-THF** and irreversible with **4**.

Single-crystal X-ray diffraction (scXRD) studies on **3** and **3-THF** confirmed that the P₄ molecule has formally inserted into the Mg–Fe bond (Figure 2). Both complexes crystallize as the *endo,exo* isomer. One of the wing-tip phosphorus atoms (P1) coordinates to iron. In the structure of **3**, the Mg atom bridges the two wing-tip P atoms, P1 and P4, with similar distances (Mg1–P1 2.6529(8) Å, Mg1–P4 2.5623(8) Å). In contrast, a THF molecule is coordinated to the magnesium atom in **3-THF**, resulting in a more asymmetric coordination environment (Mg1–P1 2.9427(8) Å, Mg1–P4 2.6320(8) Å). The P–P bond lengths are characteristic of P₄-butterfly species, revealing a short P–P bond between the bridgehead P atoms (**3**: P2–P3 2.163(1) Å; **3-THF**: P2–P3 2.1598(8) Å).^[8,11,19]



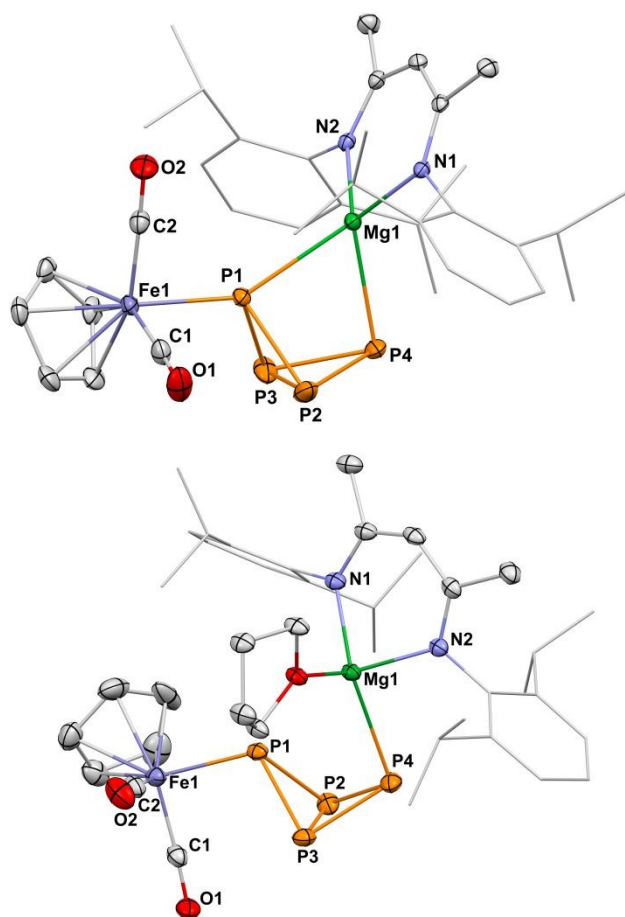


Figure 2. Solid-state molecular structures of **3** (top) and **3-THF** (bottom) measured at 123 K. Displacement ellipsoids are shown at the 30% probability level. Hydrogen atoms, non-coordinating solvent molecules and disordered groups are omitted for clarity. Selected bond lengths [Å] and angles [°] of **3**: Fe1–P1 2.3023(6), Mg1–P4 2.5623(8), Mg1–P1 2.6529(8), P1–P2 2.2188(7), P1–P3 2.2247(7), P2–P3 2.163(1), P2–P4 2.1922(9), P3–P4 2.1956(8), C1–O1 1.144(3), C2–O2 1.143(3), P1–Mg1–P4 70.55(2), N1–Mg1–N2 92.64(7). **3-THF**: Fe1–P1 2.3527(6), Mg1–P4 2.6320(8), Mg1–P1 2.9427(8), P1–P2 2.2044(7), P1–P3 2.2112(8), P2–P3 2.1598(8), P2–P4 2.2034(8), P3–P4 2.1909(8), C1–O1 1.156(3), C2–O2 1.147(3), P1–Mg1–P4 63.44(2), N1–Mg1–N2 92.16(7).

To assess the influence of substituents on the Cp ligand, we synthesized the novel $[(\text{D}^{\text{iPP}}\text{BDI})\text{MgFp}^*]$ complex **2**.[‡] Unlike **1**, complex **2** forms a dimer in the solid state via the coordination of the CO ligands to magnesium, as previously observed for related complexes.^[9,10] ^1H NMR and DOSY NMR studies reveal an equilibrium between monomeric and dimeric species in C_6D_6 solution (see Figure S71–S73). The reaction of **2** with P_4 (1 equiv.) in toluene or benzene cleanly yields **4** as a single *endo,exo*-configured product, which can be isolated in a high yield (72%) as a yellow-orange crystalline solid (Scheme 1). The molecular structure is very similar to that of **3**, as determined by scXRD studies (Figure 2). In contrast, complex **4** forms a mixture of *endo,exo* and *exo,exo* complexes when using THF. Both isomers decompose rapidly in that solvent to the symmetrical $\{[\text{Fp}^*]_2(\mu\text{-P}_4)\}$ (Figures S83 and S84, ESI), illustrating the stabilizing nature of the ion-pairing between the $[(\text{D}^{\text{iPP}}\text{BDI})\text{Mg}]^+$ cations and the $[\text{Fp}^*(\text{P}_4)]^-$ anion.

Mechanism of the P_4 insertion reaction

View Article Online

DOI: 10.1039/D6SC01230A

To gain more insight into the temperature-dependent equilibrium between **1-THF**, **3-THF** and P_4 , we performed variable-temperature (VT) $^{31}\text{P}\{^1\text{H}\}$ NMR spectroscopic measurements of **3-THF** in THF-d_8 . A van't Hoff analysis provided the thermodynamic parameters of the P_4 activation reaction ($\Delta G(298\text{ K}) = -3.9 (\pm 1.7) \text{ kJ}\cdot\text{mol}^{-1}$, $\Delta H = -37.8 (\pm 0.8) \text{ kJ}\cdot\text{mol}^{-1}$ and $\Delta S = -115 (\pm 3) \text{ J}\cdot\text{mol}^{-1}\cdot\text{K}^{-1}$; see also Table S8 and Figure S63). Exchange spectroscopy (EXSY) of the Cp signals in the ^1H NMR spectrum revealed a low activation barrier ($\Delta G^\ddagger(298\text{ K}) = 73.1 \pm 4.3 \text{ kJ}\cdot\text{mol}^{-1}$, $\Delta H^\ddagger = 16.9 \pm 2.9 \text{ kJ}\cdot\text{mol}^{-1}$, $\Delta S^\ddagger(298\text{ K}) = -188.3 \pm 10.3 \text{ J}\cdot\text{mol}^{-1}\cdot\text{K}^{-1}$; see Table S11 and Figure S69).[†] **3-THF** shows a similar behaviour in toluene- d_8 ($\Delta G(298\text{ K}) = -5.0 (\pm 6.4) \text{ kJ}\cdot\text{mol}^{-1}$, $\Delta H = -43.7 (\pm 3.1) \text{ kJ}\cdot\text{mol}^{-1}$ and $\Delta S = -129 (\pm 11) \text{ J}\cdot\text{mol}^{-1}\cdot\text{K}^{-1}$; see Table S9 and Figures S63, S64 and S76). However, in this case, the van't Hoff plot shows a nonlinear relationship between 193 K and 233 K, suggesting that the equilibrium was not reached at low temperatures. The donor-free complex $[(\text{D}^{\text{iPP}}\text{BDI})\text{MgFp}]$ (**3**) shows a similar temperature-dependent equilibrium in non-coordinating solvents (C_6D_6 or toluene- d_8).^[15] In toluene- d_8 , an additional P-containing species is observed at temperatures below 253 K besides P_4 , which we assign to the *exo,exo* isomer of **3** (Figure S79 and S80).

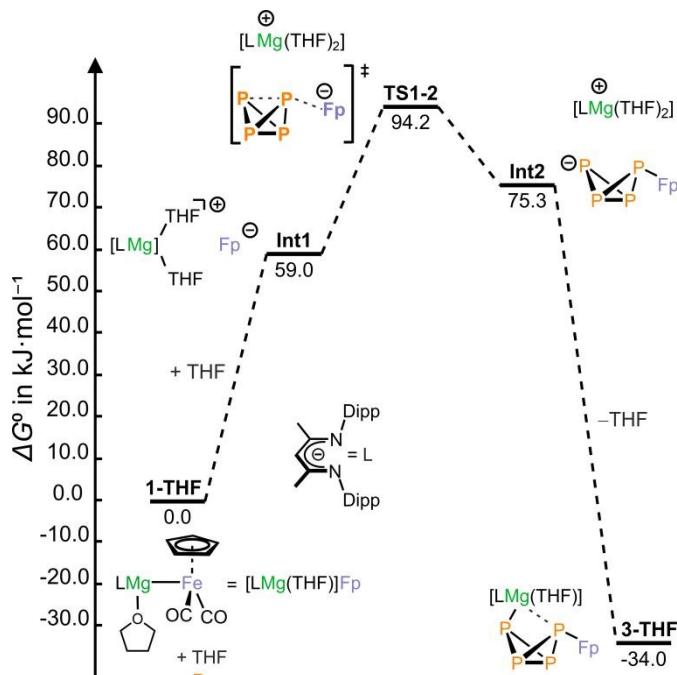


Figure 3. Computed Gibbs free energy profile for P_4 activation with **1-THF**. Relative Gibbs free energies are presented in $\text{kJ}\cdot\text{mol}^{-1}$. Level of theory: MN15/def2-TZVP/SMD(THF)//MN15/def2-SVP/SMD(THF).

DFT calculations suggest that the mechanism of the P_4 activation reaction in THF-d_8 likely involves the heterolytic cleavage of the Mg–Fe bond in compound **1-THF** (Figure 3), which appears to be barrierless (see Figure S128). The coordination of THF generates a solvent-separated ion pair consisting of the Fp^- anion and the $[(\text{D}^{\text{iPP}}\text{BDI})\text{Mg}(\text{THF})_2]^+$ cation. Fp^- attacks P_4 to form the $[\text{FpP}_4]^-$ anion, which is then trapped



by $[(\text{DippPBDI})\text{Mg}(\text{THF})_2]^+$. The Gibbs free energy (ΔG^0 and ΔG^\ddagger) profile calculated by density functional theory (DFT) for this mechanism shown in Figure 3 qualitatively agrees with the experimental data. However, the calculations slightly overestimate ΔG^0 and underestimate ΔG^\ddagger . In non-coordinating solvents such as toluene, an alternative mechanism to that depicted in Figure 3 is likely, in which the CO ligands coordinate to magnesium as previously observed in the molecular structures of magnesium-transition metal carbonylates.^[9,10] A different reaction pathway, in which P_4 coordinates to Mg, but the $[(\text{DippPBDI})\text{Mg}]$ unit does not dissociate from the Fp anion is also feasible and shows only a slightly higher activation barrier as shown by DFT calculations (see Figure S129 in the ESI). The coordination of P_4 to magnesium(II) centre has already been reported.^[18]

It is noteworthy that the complexes $[(\text{DepPBDI})\text{MgFp}(\text{THF})]$ (**5-THF**) and $[(\text{MesPBDI})\text{MgFp}(\text{THF})]$ (**6-THF**), featuring smaller Mes and Dep substituents on the BDI ligand, gave only traces of the desired P_4 -butterfly in C_6D_6 (5% and 3%, respectively), according to qualitative integration of the $^{31}\text{P}\{^1\text{H}\}$ NMR spectra (Dep = 2,6-Et₂-C₆H₃, see Table S15 and Figure S83). This indicates that the strength of the ion-pairing interaction between the Fp^- and the magnesium ion significantly influences the equilibrium. The DFT-calculated reaction energies are in full agreement with these findings, showing a greater thermodynamic preference for the formation of the P_4 -butterfly derivatives with Ar = Dipp by up to $-16.2 \text{ kJ mol}^{-1}$, compared to Ar = Dep or Mes (Table S21).†

Non-covalent interaction analysis

To investigate the influence of the cation on the thermodynamic stability, we performed a non-covalent interaction (NCI) analysis on the complexes **3**, **4** and the hypothetical complex $[\text{LiFp}^*(\mu\text{-P}_4)]$.^[21]§§ The resulting NCI and reduced wavefunction gradient (RDG) plots obtained from the wavefunction calculated at the MN15/def2-TZVP/SMD(THF)//MN15/def2-SVP/SMD(THF)^[22] level of theory are shown in Figure 4 (see also Figures S130 - S132).† Ionic interactions within compound **4** (see Figure 4 (left)) and $[\text{LiFp}^*(\mu\text{-P}_4)]$ (see Figure 4 (right)) are visualized in green to blue ($\text{sign}(\lambda_2)\rho < -0.015 \text{ a.u.}$) in the NCI isosurfaces and RDG scatter plots. The Mg cation in **4** shows a stronger interaction with the wingtip phosphorus atoms compared to the Li cation in $[\text{LiFp}^*(\mu\text{-P}_4)]$, as indicated by the dark blue color. Dispersion interactions between the $[(\text{DippPBDI})\text{Mg}]^+$ cation and $[\text{Fp}^*(\mu\text{-P}_4)]^-$ additionally stabilize the complex (Figure 4).

Thermolysis of 3-THF and photolysis of 4: synthesis of 7 and 8

Given the propensity of carbonyl complexes for the dissociation of CO,^[23] we examined the thermal and photolytic stability of **3-THF**. Upon heating of a solution in C_6D_6 to 60 °C for 5 d, **3-THF** was converted to a new species **7** (Scheme 2) characterized by an AA'BB' spin system in the $^{31}\text{P}\{^1\text{H}\}$ NMR spectrum ($\delta = 44.3 \text{ ppm}$ and 30.7 ppm , Figure S15, Table S1). It is noteworthy that the presence of the THF ligand in **3-THF** is essential for the formation of **7**, since the THF-free **3** appears to be completely stable in C_6D_6 upon heating to +60 °C and under irradiation with

a neutral white-light LED, Figure S87). In contrast, **4** is also thermally stable but rearranges upon exposure to daylight, forming complex **8** over several days (Scheme 2).

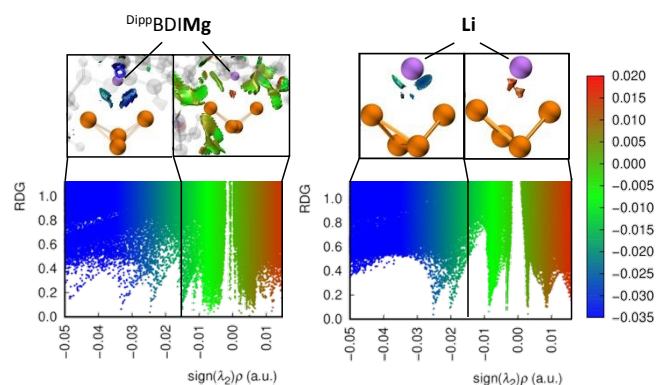
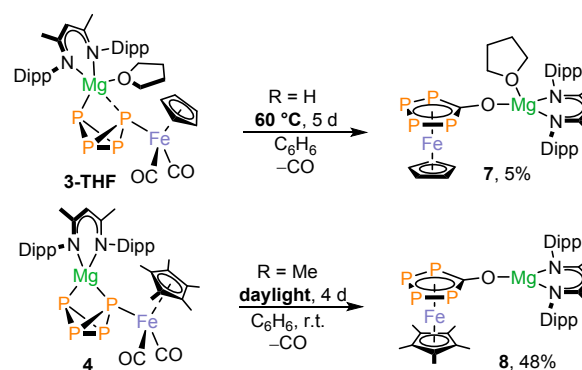


Figure 4. 3D NCI-plot and RDG scatter plot of **4** (left) and of $[\text{LiFp}^*(\mu\text{-P}_4)]$ (right). RDG scatter plot and 3D NCI-plots for ionic ($\text{sign}(\lambda_2)\rho$ range: -0.05 a.u. to -0.015 a.u.) and van der Waals region ($\text{sign}(\lambda_2)\rho$ range: -0.015 a.u. to $+0.015 \text{ a.u.}$). The repulsive interaction regions were omitted for clarity.



Scheme 2. Synthesis of **7** and **8**, r.t. = room temperature.

The $^{31}\text{P}\{^1\text{H}\}$ NMR spectrum of **8** shows an AA'XX' spin system similar to that of **7** ($\delta = 61.3$ and 36.4 ppm , see Figure 5). The scXRD analyses of **7** and **8** revealed the formation of ferrocene-like sandwich complexes with η^5 -coordinated tetraphosphacyclopentadienolate ligands. The planar $\text{P}_4\text{C}(\text{O})$ rings are eclipsed with respect to the co-planar Cp or Cp* moiety. The P–P and P–C bond lengths indicate a delocalized bonding situation (**7**: P–P 2.1013(8) to 2.124(1) Å, P–C 1.786(2) and 1.790(2) Å; **8**: P–P 2.100(2) to 2.135(2) Å, P–C 1.781(5) and 1.785(6) Å). Complex **7** crystallizes as a monomer while the THF-free compound **8** forms a polymeric structure via coordination of the P2 atom to a $[(\text{DippPBDI})\text{Mg}]^+$ cation of an adjacent molecule (Mg1–P2 2.793(2) Å, Figure S93). To our knowledge, **7** and **8** are the first complexes featuring η^5 -coordinated tetraphosphacyclopentadienolate $\text{P}_4\text{C}(\text{O})^-$ ligands. A similar CO insertion resulting in an η^5 - $\text{P}_4\text{C}(\text{O})$ ligand has been observed for the reaction of $[\text{Fe}_2(\text{CO})_9]$ with $(\text{Cp}^*\text{Fe})_2(\mu\text{-P}_4)$ ($\text{Cp}^* = \text{C}_5\text{H}_2^+\text{Bu}_3$), which affords the oligonuclear complex $\{[\text{Cp}^*\text{Fe}(\text{CO})_2]_2(\mu_4, \eta^3\text{-}1:1:1\text{-P}_4\text{CO})\{\text{Fe}(\text{CO})_4\}\{\text{Fe}(\text{CO})_3\}\}$.^[24] Additionally, a few related tetraphospholide complexes are known which display similar P–P bond lengths, e.g. $[\text{Cp}^*\text{Fe}(\eta^5\text{-P}_4\text{C}^t\text{Bu})]$,^[25] $[\text{Cp}^*\text{Fe}(\text{P}_4\text{SiL})]$ (L = PhC(N^tBu)₂),^[26]



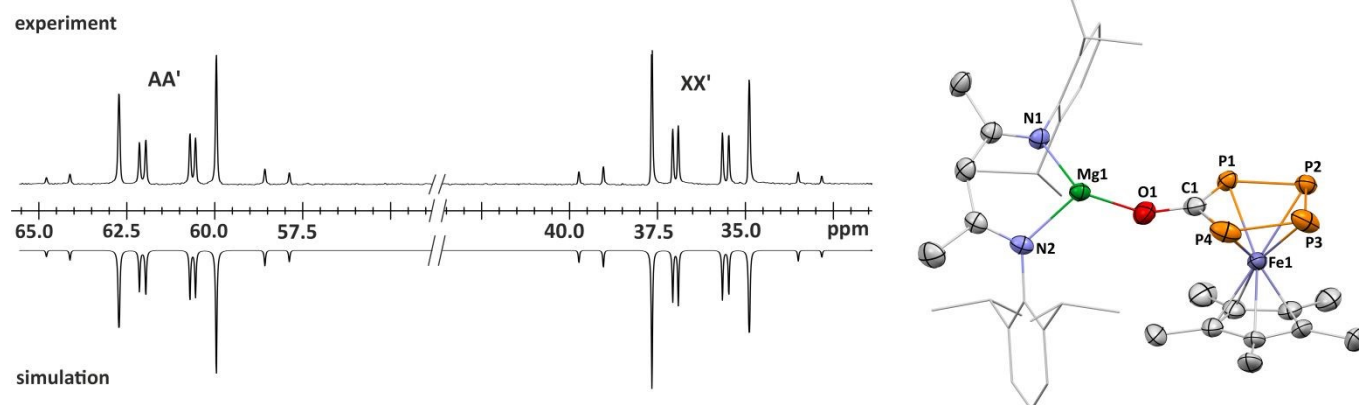


Figure 5. Experimental (upwards) and simulated (downwards) $^{31}\text{P}\{^1\text{H}\}$ NMR spectrum of **7** (left) and its solid-state molecular structure measured at 123 K (right). The solid-state molecular structure and the $^{31}\text{P}\{^1\text{H}\}$ NMR spectrum of **8** are similar and therefore displayed in the ESI. Displacement ellipsoids are shown at the 30% probability level. Hydrogen atoms are omitted, and the Dipp groups are shown in wireframe representation for clarity. Selected bond length [Å] and angles [°]: P3–P4 2.100(2), P1–P2 2.112(2), P2–P3 2.135(2), P1–C1 1.781(5), P4–C1 1.785(6), C1–O1 1.309(5), Fe–P 2.345(1) – 2.361(2), Fe1–C1 2.231(4), C1–O1–Mg1 145.8(3), P4Ccentroid–Fe1–C5-centroid 174.1

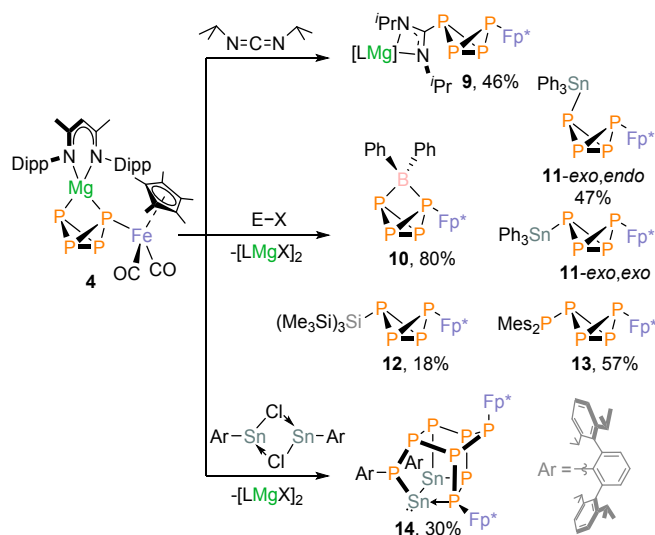
Reactivity of **4** towards electrophiles

The high-yielding synthesis of complex **4** enabled us to investigate its reactivity towards electrophiles in detail. During these studies, we found that **4** reacts readily and selectively with numerous electrophiles, including main-group element halides and heterocumulenes (Scheme 3). The products exhibit characteristic AMX_2 spin systems in the $^{31}\text{P}\{^1\text{H}\}$ NMR spectra, which provide evidence for P-functionalized P_4 butterfly compounds. Using bulky electrophiles such as $^i\text{PrNCN}^i\text{Pr}$, Ph_2BCl , Ph_3SnCl , $(\text{Me}_3\text{Si})_3\text{SiCl}$, and Mes_2PCl we were able to isolate the new P_4 -butterfly complexes **9–13**. Complexes **9**, **10** and **12** are stable in solution for several days, while **11** and **13**

similar dimerization reaction for the pentaphospane $\text{P}_5(\text{C}_6\text{F}_5)_2$ generated from $(\text{DippPBDI})\text{GaP}_4$ butterfly with $(\text{C}_6\text{F}_5)_2\text{PBr}$.^[29]

ScXRD studies revealed the molecular structures of **9–13**. Complex **9** results from an insertion of the carbodiimide $^i\text{PrNCN}^i\text{Pr}$ into the Mg–P bond of **4**. The two nitrogen atoms coordinate to magnesium, and the carbon atom is bound to phosphorus (Figure 6). For **9**, **12**, and **13** (Figure S1), the butterfly- P_4 unit is an *exo,exo* configuration with the Fp^* and carbodiimide, $(\text{Me}_3\text{Si})_3\text{Si}$ - and Mes_2P -substituents pointing toward the bridgedhead P atoms. In contrast, complex **10** shows a symmetrically bridging Ph_2B moiety (P–B 2.016(2) Å and 2.055(2) Å). An *endo,exo* configuration is likewise observed for the Ph_3Sn -substituted complex **11**.

The $^{31}\text{P}\{^1\text{H}\}$ NMR data are consistent with these crystallographic findings. For complex **9**, the $^2J_{\text{PP}}$ coupling (258 Hz) is larger than the $^1J_{\text{PP}}$ couplings (179 Hz, 185 Hz), indicating an *exo,exo* butterfly structure in solution. The $^{13}\text{C}\{^1\text{H}\}$ NMR spectrum displays a doublet of doublet for the quaternary carbon atom of the carbodiimide unit due to C–P coupling ($\delta = 175.0$ ppm, $^1J_{\text{PC}} = 103.9$ Hz, $^3J_{\text{PC}} = 23.3$ Hz, Figure S21). The *exo,exo* isomer is also present for **12** and **13**, as evidenced by the high-field shifted P_M resonances of the AMX_2 spin systems and large $^2J_{\text{PP}}$ couplings ($^2J_{\text{AM}} = 235$ Hz and 259 Hz, respectively; see Tables S5 and S6), which result from through-space interactions of the lone pairs.^[10] Additionally ^{29}Si satellites ($^1J_{\text{SiP}} = 97.5$ Hz) were detected for the P atom with the $(\text{Me}_3\text{Si})_3\text{Si}$ substituent. In contrast, the small $^2J_{\text{PP}}$ coupling constant ($^2J_{\text{AM}} = 33$ Hz) indicates that compound **10** retains the *endo,exo* configuration in solution. The resonances assigned to the wingtip phosphorus atoms P1 and P4 exhibit chemical shifts similar to compound **4**, while the signal of the bridgehead phosphorus atoms P2 and P3 is shifted downfield by 50.4 ppm. The $^{11}\text{B}\{^1\text{H}\}$ NMR spectrum shows a broad signal ($\Delta\nu_{1/2} = 362$ Hz) at 20.5 ppm with unresolved coupling to phosphorus. The $^{31}\text{P}\{^1\text{H}\}$ NMR spectra of the Ph_3Sn -substituted complex **11** display two distinct AMX_2 spin systems in an approximate 1:1 integral ratio,



Scheme 3. Reactivity of **6** towards selected electrophiles.

gradually decompose at ambient temperature (Figures S54 and S84). It is noteworthy that **11** dimerises slowly to a tricyclic P_8 cluster **15**, as revealed by ^{31}P NMR data and a preliminary scXRD analysis (Figure S48). Weigand and co-workers observed a



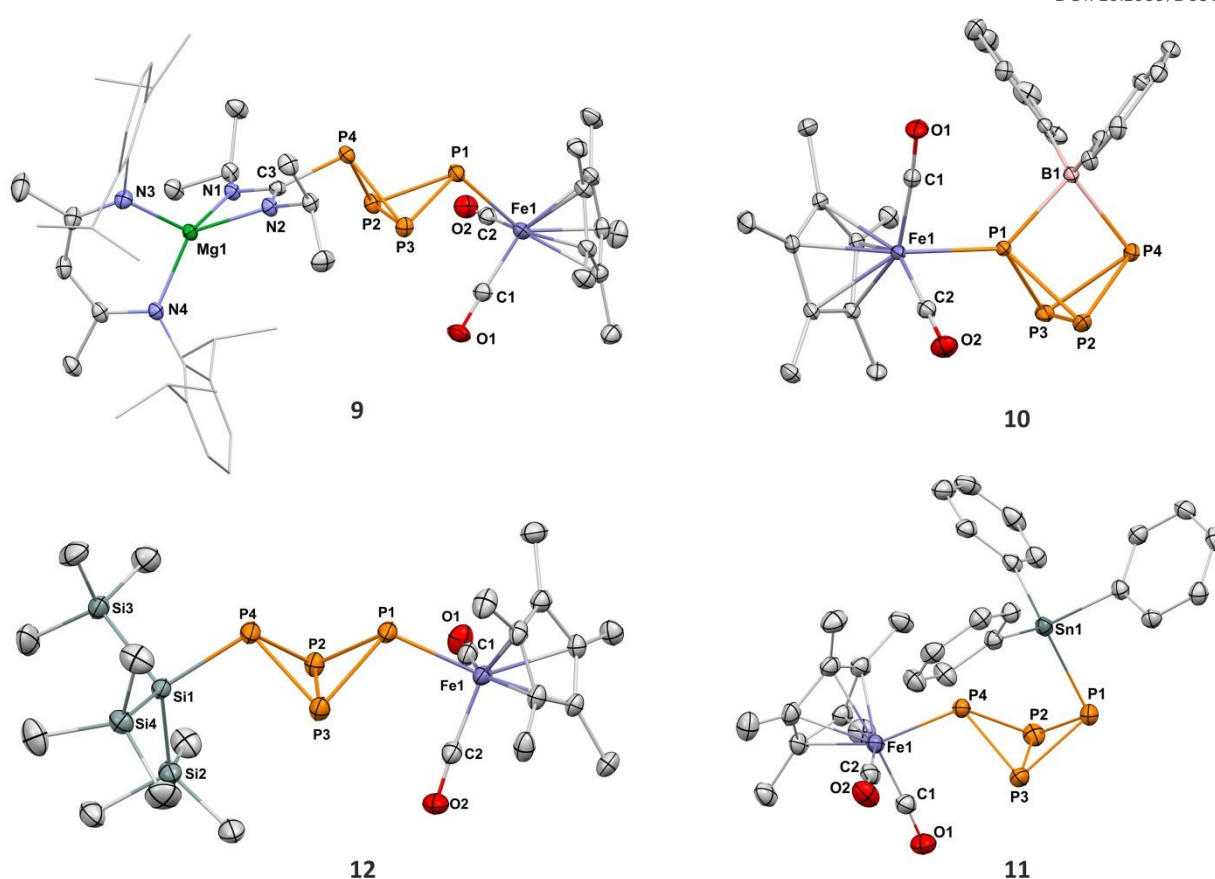


Figure 6. Solid state molecular structures of **9**, **10**, **11** and **12** measured at 123 K. Displacement ellipsoids are shown at the 30% probability level. Hydrogen atoms, non-coordinating solvent molecules and disordered groups are omitted for clarity. The Dipp groups in **7** are depicted in tube-like model for clarity. Selected bond length[Å] and angles [°] are for **9**: Fe1–P1 2.3064(6), P1–P2 2.2169(6), P1–P3 2.2286(7), P2–P3 2.1795(7) P2–P4 2.2119(7), P3–P4 2.2083(7), P4–C3 1.889(2), C1–O1 1.148(2), C2–O2 1.147(2), N2–C3 1.332(2), N1–C3 1.335(2), N1–C3–N2 114.4(2), N3–Mg1–N4 94.24(7). **10**: Fe1–P1 2.2434(4), P1–B1 2.016(2), P4–B1 2.055(2), P1–P2 2.2063(6), P1–P3 2.2035(5), P2–P3 2.1974(7), P3–P4 2.2100(6), P2–P4 2.2108(7), C1–O1 1.145(2), C2–O2 1.142(2), P1–B1–P4 83.67(7), Fe1–P1–B1 134.90(5). **11**: Fe1–P4 2.2734(7), Sn1–P1 2.5675(7), P1–P2 2.2063(9), P1–P3 2.2080(9), P2–P3 2.179(1), P2–P4 2.2233(9), P3–P4 2.2060(9), C1–O1 1.147(3), C2–O2 1.149(3). Second molecule in asymmetric unit: Fe1–P4 2.2848(7), Sn1–P1 2.5549(7), P1–P2 2.206(1), P1–P3 2.208(1), P2–P4 2.2261(9), P3–P4 2.2084(9), C1–O1 1.145(3), C2–O2 1.145(3). **12**: Fe1–P1 2.294(1), P4–Si 2.294(1), P1–P2 2.218(1), P1–P3 2.231(2), P3–P4 2.217(1), P2–P3 2.167(1), P2–P4 2.214(1), C1–O1 1.152(5), C2–O2 1.144(5), Si1–P4–P3 101.91(5), P1–P3–P4 81.98(5), Fe1–P1–P3 109.49(5).

indicating that the *endo,exo* and *exo,exo* isomers coexist in solution (Figure S30). However, when a sample of isolated **11** was dissolved at $-80\text{ }^{\circ}\text{C}$ in toluene- d_8 and the $^{31}\text{P}\{^1\text{H}\}$ NMR was recorded at $-80\text{ }^{\circ}\text{C}$, only the signals of the *endo,exo* isomer were observed ($^2J_{\text{AM}} = 16\text{ Hz}$, Table S3). Variable-temperature $^{31}\text{P}\{^1\text{H}\}$ NMR spectroscopy of **11** shows a slow conversion to an equilibrium mixture of the *endo,exo* and *exo,exo* isomer at elevated temperature (Figure S81). The ^{119}Sn NMR spectrum of *endo,exo* **11** dissolved at $-80\text{ }^{\circ}\text{C}$ shows a doublet of doublets with a $^1J_{\text{Psn}}$ coupling of 973 Hz and a smaller coupling of $^1J_{\text{SnP}} = 299\text{ Hz}$ in agreement with the $^{117/119}\text{Sn}$ -P coupling constants derived from the $^{31}\text{P}\{^1\text{H}\}$ NMR spectrum (see Table S3). The reactivity of **4** towards electrophiles strongly depends on the nature and steric bulk of the electrophile. The substituents must provide sufficient steric protection to stabilize the resulting butterfly complex without suppressing reactivity. Thus, $^{31}\text{P}\{^1\text{H}\}$ NMR spectroscopic monitoring studies indicate that **4** cleanly reacts with the moderately bulky electrophile Me_3SiBr to afford the desired P_4 -butterfly compound

$\text{Fp}^*(\mu\text{-P}_4)\text{SiMe}_3$. However, this compound is unstable and decomposes overnight at room temperature. In contrast, the reaction of the bulkier $^t\text{BuMe}_2\text{SiCl}$ with **4** is slow, resulting in an incomplete substitution reaction. Oxidizing electrophiles such as $(2,6\text{-Mes}_2\text{-C}_6\text{H}_3)\text{PCl}_2$ (Mes = $\text{C}_6\text{H}_2\text{-2,4,6-Me}_3$) produce Fp^*_2P_4 and P_4 among other decomposition products.

The reaction of **4** with $[\text{ArSnCl}]_2$ (0.5 equiv., Ar = 2,6-Dipp $_2$ - C_6H_3 , Dipp = 2,6- $^i\text{Pr}_2$ - C_6H_3) affords the polycyclic compound **14** (Figure 7a), which formally is the dimerization product of the expected P_4 -butterfly species $\text{Fp}^*(\mu\text{-P}_4)\text{SnAr}$. The molecular structure of **14** consists of a pentacyclo[5.2.1.0 2,6 .0 3,9 .0 4,8]decane-like P_8Sn_2 core derived from a norbornane-like P_7 moiety with an exocyclic ArP unit and a Sn–Sn single bond (2.8591(2) Å).^[30] The P–P bond lengths (2.1747(6)–2.2483(6) Å) are in the range of P–P single bonds. Notably, the Sn1–P1 bond length 2.6726(4) Å results from a dative interaction involving the lone pair of P1.



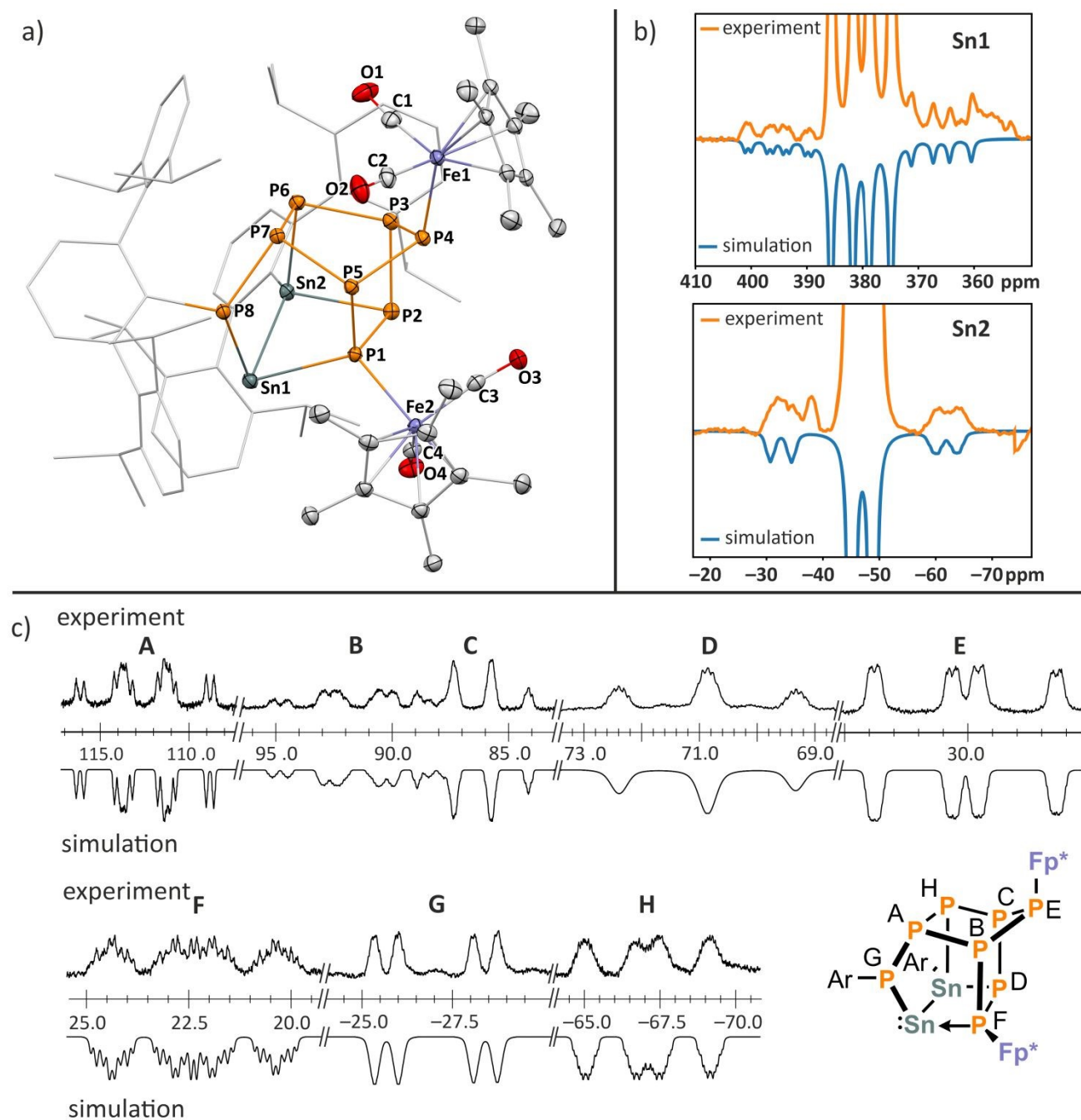
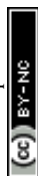


Figure 7. a) Solid-state molecular structure of **14** measured at 123 K. Displacement ellipsoids are shown at the 30% probability level. Hydrogen atoms are omitted for clarity. Selected bond length [Å] and angles [°]: Sn1–Sn2 2.8591(2), Sn1–P1 2.6726(4), Sn1–P8 2.5967(4), Sn2–P2 2.5968(4), Sn2–P6 2.5707(4), P1–P2 2.2644(6), P1–P5 2.2191(6), P2–P3 2.2015(6), P3–P4 2.1950(6), P3–P6 2.2483(6), P4–P5 2.1747(6), P5–P7 2.2054(6), P6–P7 2.2337(6), P7–P8 2.2008(6), Sn1–Sn2–P2 89.673(10), P1–Sn1–Sn2 74.309(9), P6–Sn2–Sn1 106.62(1). b) $^{119}\text{Sn}\{^1\text{H}\}$ experimental NMR spectrum (224 MHz, 298 K, C_6D_6) (top) and simulation (bottom). An exponential window function (WDW EM) with a line broadening of 50 Hz has been used. The baseline has been corrected using a multipoint spline with the “basl” and “sab” commands in Bruker TopSpin 4.20. c) $^{31}\text{P}\{^1\text{H}\}$ experimental spectrum (162 MHz, 298 K, C_6D_6) (top) and simulation (bottom).

The remaining Sn–P distances are in a close range (2.5707(4)–2.5967(4) Å), consistent with Sn–P single bonds. The structural framework of **14** is reminiscent of bishomocubanes derived from dimethyl dicyclopentadienedicarboxylate (Thiele’s ester).^[31] Additionally, some related carbocyclic polyphosphanes have been described, resulting from the dimerization of 1,2,4-triphosphacyclopenta-1,3-dienes or the

reaction of R_3Sn stabilized 1,2,4-triphosphacyclopenta-1,3-dienes with *tert*-butylphosphaalkyne.^[32] Notably, the dimerization of the As_4 -butterfly complexes $[\{\text{Cp}^*\text{Fe}(\text{CO})_2\}_2(\mu, \eta^{1:1}\text{-As}_4)]$ or $[\{\text{Cp}^*\text{Cr}(\text{CO})_3\}_2(\mu, \eta^{1:1}\text{-As}_4)]$ afford realgar-like (tricyclo[3.3.0.0^{3,7}]octane)- As_8 species.^[33] Similar realgar-like P_8 units are also known.^[34]



The ^{119}Sn NMR spectrum of **14** shows an apparent doublet of doublets at 380 ppm, and a broad doublet ($\Delta\nu_{\%} > 700$ Hz) with unresolved fine structure at -47 ppm. The assignment of the Sn1 and Sn2 signals is based on the calculated $^1\text{J}_{^{119}\text{Sn}-^{31}\text{P}}$ coupling constants of 1471 Hz for Sn1-P8, 970 Hz for Sn1-P1 and 823 Hz for Sn2-P6 (Figure 7b; see ESI, section 8.3 for details). These data compare well with the experimental values of 1540 Hz, 882 Hz and 830 Hz, respectively. The ^{117}Sn and ^{119}Sn satellites could be detected in the ^{119}Sn NMR spectrum ($^1\text{J}_{^{119}\text{Sn}1-^{119}\text{Sn}2} \approx 6700$ Hz; calculated -7663 Hz), confirming that the Sn-Sn bond remains intact in solution. For comparison, the $^1\text{J}_{^{119}\text{Sn}-^{119}\text{Sn}}$ coupling constants in $\text{Ar}^*\text{SnSnPh}_2\text{Ar}^*$ ($\text{Ar}^* = \text{C}_6\text{H}_3-2,6-(\text{C}_6\text{H}_2-2,4,6\text{-}i\text{Pr}_3)$ and $\text{Ar}^*\text{SnSn}(\text{Me}_2)\text{Ar}^*$ are 7237 Hz and 8330 Hz, respectively.^[35]

The $^{31}\text{P}\{^1\text{H}\}$ NMR spectrum of **14** displays a set of eight multiplets between 112.4 ppm and -67.1 ppm for the eight distinct P-atoms. The coupling constants were determined by simulating the spectrum using an iterative fitting procedure (Figure 7c and Table S7, ESI). Compound **14** is unstable in solution at ambient temperature. Upon storing a solution at room temperature, the signals of **14** gradually disappear over the course of three weeks, and two new sets of signals appear in the $^{31}\text{P}\{^1\text{H}\}$ NMR spectrum in the same chemical shift range as for **14**, indicating that it rearranges slowly in solution to form a new complex **16** (see ESI, Figure S60). A preliminary scXRD analysis shows that **14** eliminates one CO ligand and binds to two adjacent phosphorus atoms (Figure S49). Based on the very similar chemical shifts and coupling constants in the ^{119}Sn and $^{31}\text{P}\{^1\text{H}\}$ NMR spectra (Figure S57 and S60), we assume that two isomers of **16** coexist in solution.†

Conclusions

We have shown that the inorganic Grignard reagents **1** and **2** effectively activate P_4 through furnishing P_4 -butterfly dianions that are coordinated by Fe and the bulky β -diketiminato magnesium cation $[(^{\text{Dipp}}\text{PBDI})\text{Mg}]^+$. Our theoretical analysis emphasizes the importance of non-covalent and dispersion interactions in stabilizing these complexes, which appear to be stronger for $[(^{\text{Dipp}}\text{PBDI})\text{Mg}]^+$ than for Li^+ .§§ The reversible dissociation of the Fe-Mg Lewis pairs **1** and **2** into solvent-separated ion pairs appears to be key. According to DFT calculations, the reactions proceed stepwise via nucleophilic attack by the Fp^- or Fp^{*-} anion P_4 and subsequent coordination to $[(^{\text{Dipp}}\text{PBDI})\text{Mg}]^+$. However, unlike previous studies, these reactions do not require an external Lewis acid, simplifying reactivity investigations. Reactions of **4** with electrophiles generate a variety of new mixed substituted P_4 -butterfly species **9-13**, as well as the novel Sn_2P_8 cluster **14**. Additionally, thermally or photochemically induced rearrangements led to rare tetraphosphole complexes **7** and **8**.

Our results indicate that combining transition-metalate anions with the $[(^{\text{Dipp}}\text{PBDI})\text{Mg}]^+$ cation is a promising strategy for deliberate and selective P_4 activation and functionalization. When sufficient steric bulk is provided, the resulting P_4 -butterfly complexes can be easily isolated, marking an ideal starting point for future reactivity studies. In other cases, dimerization to P_8

frameworks can be observed. Ongoing work in our group focuses on the reaction chemistry of complexes **9-14** and on the broader applicability of our approach using a wider range of metal-based Lewis pairs.

Author contributions

F. G. conceptualisation, investigation – synthesis and characterisation, writing – original draft; J. B. investigation - DFT studies of the mechanism and NCI analysis; W. M. S. investigation – DOSY and EXSY studies; F. W. investigation – Sn NMR studies and DFT calculations; R. W., G. B. conceptualisation, supervision; R.W., R. G., H. Z. supervision and funding acquisition. All authors contributed to manuscript review, editing and discussion.

Conflicts of interest

There are no conflicts to declare.

Data availability

The data supporting the findings of this work is available in the main text or the electronic supplementary information. Primary research data for this work is openly accessible on Radar4Chem (<https://radar4chem.radar-service.eu/radar/de/home>) under the DOI: 10.22000/7wa7f1kdq20s260j. Crystallographic Information Files (CIFs) have been deposited at the CCDC under the deposition numbers 2529860-2529874 (see ESI). These data are provided free of charge by the joint Cambridge Crystallographic Data Center and Fachinformationszentrum Karlsruhe Access Structures service.

Acknowledgements

We thank the Deutsche Forschungsgemeinschaft for funding (RTG 2620 Ion Pair Effects in Molecular Reactivity, project number 426795949). J. B. and H. Z. acknowledge the computational and data resources provided by the Leibniz Supercomputing Centre (www.lrz.de).

Notes and references

‡ The Fp^{*-} anion in **2** is more electron-rich, which should favour the insertion product as demonstrated for the reaction of KFp^* with CO_2 .^[36]

§ Complex **2** forms an Mg-OC-Fe bonded monomer upon crystallization from DME (Figure S103) and a dimer with similar Mg-OC-Fe linkages upon crystallization from toluene (Figure S101). Additionally, monomeric Mg-Fe-bonded structures have been obtained for **5-THF** and **6-THF** by crystallization from THF (Figures S99 and S100). In line with previous results by Mountford and co-workers, these data indicate that the aggregation is reversible, depending on the solvent and the crystallization conditions.^[14]

§§ Lammertsma and co-workers have demonstrated that the reaction of LiFp^* and P_4 in THF affords a mixture of iron polyphosphides.^[12]



- [1] a) D. Corbridge, *Phosphorus. Chemistry, Biochemistry and Technology, Sixth Edition*, CRC Press, **2013**; b) M. A. de Boer, L. Wolzak, J. C. Slootweg in *Phosphorus Recovery and Recycling* (Hrsg.: H. Ohtake, S. Tsuneda), Springer Singapore, Singapore, **2019**, S. 75–100; c) N. Weferling, S. M. Zhang, C. H. Chiang, *Procedia Eng.* **2016**, *138*, 291.
- [2] a) S. Hauer, T. M. Horsley Downie, G. Balázs, K. Schwedtmann, J. J. Weigand, R. Wolf, *Angew. Chem. Int. Ed.* **2024**, *63*, e202317170; b) F. Dielmann, M. Elsayed Moussa, C. Riesinger, M. Scheer, *Z. Anorg. Allg. Chem.* **2024**, *650*; c) S. Reichl, E. Mädl, F. Riedlberger, M. Piesch, G. Balázs, M. Seidl, M. Scheer, *Nat. Commun.* **2021**, *12*, 5774; d) S. Reichl, F. Riedlberger, M. Piesch, G. Balázs, M. Seidl, M. Scheer, *Chem. Sci.* **2023**, *14*, 7285; e) M. Peruzzini, L. Gonsalvi, A. Romerosa, *Chem. Soc. Rev.* **2005**, *34*, 1038; f) B. M. Cossairt, N. A. Piro, C. C. Cummins, *Chem. Rev.* **2010**, *110*, 4164; g) M. Caporali, L. Gonsalvi, A. Rossin, M. Peruzzini, *Chem. Rev.* **2010**, *110*, 4178; h) C. M. Hoidn, D. J. Scott, R. Wolf, *Chem. Eur. J.* **2021**, *27*, 1886; i) L. Giusti, V. R. Landaeta, M. Vanni, J. A. Kelly, R. Wolf, M. Caporali, *Coord. chem. rev.* **2021**, *441*, 213927; j) K. Trabitsch, S. Hauer, K. Schwedtmann, P. Royla, J. J. Weigand, R. Wolf, *Inorg. Chem. Front.* **2025**, *12*, 2013; k) M. Scheer, G. Balázs, A. Seitz, *Chem. Rev.* **2010**, *110*, 4236.
- [3] a) O. J. Scherer, G. Schwarz, G. Wolmershäuser, *Z. anorg. allg. chem.* **1996**, *622*, 951; b) S. Pelties, D. Herrmann, B. de Bruin, F. Hartl, R. Wolf, *Chem. Commun.* **2014**, *50*, 7014; c) D. W. Agnew, C. E. Moore, A. L. Rheingold, J. S. Figueroa, *Angew. Chem. Int. Ed.* **2015**, *54*, 12673; d) M. J. Drance, S. Wang, M. Gembicky, A. L. Rheingold, J. S. Figueroa, *Organometallics* **2020**, *39*, 3394; e) M. Haimerl, C. Graßl, M. Seidl, M. Piesch, M. Scheer, *Chem. Eur. J.* **2021**, *27*, 18129; f) S. Heinel, S. Reisinger, C. Schwarzmaier, M. Bodensteiner, M. Scheer, *Angew. Chem. Int. Ed.* **2014**, *53*, 7639; g) R. J. Schwamm, M. Lein, M. P. Coles, C. M. Fitchett, *Angew. Chem. Int. Ed.* **2016**, *55*, 14798; h) J. Haberstroh, C. Taube, J. Fidelius, S. Schulz, N. Israel, E. Dmitrieva, R. M. Gomila, A. Frontera, R. Wolf, K. Schwedtmann et al., *Chem. Commun.* **2024**, *60*, 8537; i) I. Kovács, G. Baum, G. Fritz, D. Fenske, N. Wiberg, H. Schuster, K. Karaghiosoff, *Z. anorg. allg. chem.* **1993**, *619*, 453; j) S. Khan, R. Michel, J. M. Dieterich, R. A. Mata, H. W. Roesky, J.-P. Demers, A. Lange, D. Stalke, *J. Am. Chem. Soc.* **2011**, *133*, 17889.
- [4] a) Y. Xiong, S. Yao, M. Brym, M. Driess, *Angew. Chem. Int. Ed.* **2007**, *46*, 4511; b) J. W. Dube, C. M. E. Graham, C. L. B. Macdonald, Z. D. Brown, P. P. Power, P. J. Ragona, *Chem. Eur. J.* **2014**, *20*, 6739; c) C. M. E. Graham, C. L. B. Macdonald, P. P. Power, Z. D. Brown, P. J. Ragona, *Inorg. Chem.* **2017**, *56*, 9111; d) G. Prabusankar, A. Doddi, C. Gemel, M. Winter, R. A. Fischer, *Inorg. Chem.* **2010**, *49*, 7976; e) D. Reiter, P. Frisch, D. Wendel, F. M. Hörmann, S. Inoue, *Dalton trans.* **2020**, *49*, 7060; f) M. D. Roy, A. Heilmann, M. A. Ellwanger, S. Aldridge, *Angew. Chem. Int. Ed.* **2021**, *60*, 26550; g) D. Sarkar, C. Weetman, D. Munz, S. Inoue, *Angew. Chem. Int. Ed.* **2021**, *60*, 3519; h) P. Dabringhaus, T. Heizmann, I. Krossing, *Chem. Eur. J.* **2023**, *29*, e202302212; i) D. Holschumacher, T. Bannenber, K. Ibrom, C. G. Daniliuc, P. G. Jones, M. Tamm, *Dalton trans.* **2010**, *39*, 10590; j) J. J. Weigand, M. Holthausen, R. Fröhlich, *Angew. Chem. Int. Ed.* **2009**, *48*, 295.
- [5] M. Baudler, C. Adamek, S. Opiela, H. Budzikiewicz, D. Ouzounis, *Angew. Chem. Int. Ed.* **1988**, *27*, 1059.
- [6] a) M. M. Rauhut, A. M. Semsel, *J. Org. Chem.* **1963**, *28*, 471; b) M. M. Rauhut, A. M. Semsel, *J. Org. Chem.* **1963**, *28*, 473; c) M. M. Rauhut, R. Bernheimer, A. M. Semsel, *J. Org. Chem.* **1963**, *28*, 478.
- [7] K. X. Bhattacharyya, S. Dreyfuss, N. Saffon-Merceron, N. Mézailles, *Chem. Commun.* **2016**, *52*, 5179.
- [8] J. E. Borger, A. W. Ehlers, M. Lutz, J. C. Slootweg, K. Lammertsma, *Angew. Chem. Int. Ed.* **2014**, *53*, 12836.
- [9] J. E. Borger, M. S. Bakker, A. W. Ehlers, M. Lutz, J. C. Slootweg, K. Lammertsma, *Chem. Commun.* **2016**, *52*, 3284.
- [10] J. E. Borger, A. W. Ehlers, M. Lutz, J. C. Slootweg, K. Lammertsma, *Angew. Chem. Int. Ed.* **2017**, *56*, 285.
- [11] J. E. Borger, A. W. Ehlers, M. Lutz, J. C. Slootweg, K. Lammertsma, *Angew. Chem. Int. Ed.* **2016**, *55*, 613.
- [12] J. E. Borger, M. K. Jongkind, A. W. Ehlers, M. Lutz, J. C. Slootweg, K. Lammertsma, *ChemistryOpen* **2017**, *6*, 350.
- [13] a) C. G. P. Ziegler, T. M. Maier, S. Pelties, C. Taube, F. Hennersdorf, A. W. Ehlers, J. J. Weigand, R. Wolf, *Chem. Sci.* **2019**, *10*, 1302; b) C. G. P. Ziegler, C. Taube, J. A. Kelly, G. Hierlmeier, M. Uttendorfer, J. J. Weigand, R. Wolf, *Chem. Commun.* **2020**, *56*, 14071; c) Y. Liu, F. F. Westermair, I. Becker, S. Hauer, M. Bodensteiner, C. Hennig, G. Balázs, F. Meyer, R. M. Gschwind, R. Wolf, *J. Am. Chem. Soc.* **2025**, *147*, 7083; d) M. D. Fritz, J. A. Kelly, G. Balázs, R. Wolf, *ChemistryEurope* **2025**.
- [14] M. P. Blake, N. Kaltsoyannis, P. Mountford, *Chem. Commun.* **2013**, *49*, 3315.
- [15] M. Garçon, C. Bakewell, A. J. P. White, M. R. Crimmin, *Chem. Commun.* **2019**, *55*, 1805.
- [16] a) H. Felkin, P. J. Knowles, B. Meunier, A. Mitschler, L. Ricard, R. Weiss, *J. Chem. Soc., Chem. Commun.* **1974**, *44*; b) J. A. Kelly, J. Gramüller, R. M. Gschwind, R. Wolf, *Dalton trans.* **2021**, *50*, 13985; c) M. Gawron, F. Gilch, D. Schmidhuber, J. A. Kelly, T. M. Horsley Downie, A. Jacobi von Wangelin, J. Rehbein, R. Wolf, *Angew. Chem. Int. Ed.* **2024**, *63*, e202315381; d) V. R. Landaeta, T. M. Horsley Downie, R. Wolf, *Chem. Rev.* **2024**, *124*, 1323.
- [17] a) M. Arrowsmith, M. S. Hill, A. L. Johnson, G. Kociok-Köhn, M. F. Mahon, *Angew. Chem. Int. Ed.* **2015**, *54*,



- 7882; b) S. Thum, O. P. E. Townrow, J. Langer, S. Harder, *Chem. Sci.* **2025**, *16*, 4528.
- [18] M. J. Evans, D. T. Nguyen, J. M. Parr, J. Mullins, R. Mondal, T. Rajeshkumar, L. Maron, C. Jones, *Chem* **2025**, 102650.
- [19] J. Bresien, K. Faust, C. Hering-Junghans, J. Rothe, A. Schulz, A. Villinger, *Dalton Trans.* **2016**, *45*, 1998.
- [20] D. C. Meier, Á. García-Romero, D. González-Pinardo, N. H. Rees, A. Lovstedt, I. Fernández, J. M. Goicoechea, *Chem. Sci.* **2025**.
- [21] J. Contreras-García, E. R. Johnson, S. Keinan, R. Chaudret, J.-P. Piquemal, D. N. Beratan, W. Yang, *J. Chem. Theory Comput.* **2011**, *7*, 625.
- [22] a) H. S. Yu, X. He, S. L. Li, D. G. Truhlar, *Chem. Sci.* **2016**, *7*, 6278; b) F. Weigend, R. Ahlrichs, *Phys. Chem. Chem. Phys.* **2005**, *7*, 3297; c) A. V. Marenich, C. J. Cramer, D. G. Truhlar, *J. Phys. Chem. B* **2009**, *113*, 6378.
- [23] a) J. J. Turner, M. W. George, M. Poliakoff, R. N. Perutz, *Chem. Soc. Rev.* **2022**, *51*, 5300; b) O. J. Scherer, T. Hilt, G. Wolmershäuser, *Organometallics* **1998**, *17*, 4110; c) O. J. Scherer, T. Brück, G. Wolmershäuser, *Chem. Ber.* **1988**, *121*, 935; d) M. Scheer, U. Becker, *J. Organomet. Chem.* **1997**, *545-546*, 451; e) O. J. Scherer, R. Winter, G. Wolmershäuser, *Z. Anorg. Allg. Chem.* **1993**, *619*, 827; f) C. Eichhorn, O. J. Scherer, T. Sögding, G. Wolmershäuser, *Angew. Chem. Int. Ed.* **2001**, *40*, 2859; g) O. J. Scherer, J. Schwalb, G. Wolmershäuser, W. Kaim, R. Gross, *Angew. Chem. Int. Ed.* **1986**, *25*, 363.
- [24] R. Grünbauer, C. Schwarzmaier, M. Eberl, G. Balázs, M. Scheer, *Inorg. Chim. Acta* **2021**, *518*, 120234.
- [25] M. Scheer, S. Deng, O. J. Scherer, M. Sierka, *Angew. Chem. Int. Ed.* **2005**, *44*, 3755.
- [26] R. Yadav, T. Simler, S. Reichl, B. Goswami, C. Schoo, R. Köppe, M. Scheer, P. W. Roesky, *J. Am. Chem. Soc.* **2020**, *142*, 1190.
- [27] J. A. Kelly, V. Streitferdt, M. Dimitrova, F. F. Westermair, R. M. Gschwind, R. J. F. Berger, R. Wolf, *J. Am. Chem. Soc.* **2022**, *144*, 20434.
- [28] A. S. Ionkin, W. J. Marshall, B. M. Fish, A. A. Marchione, L. A. Howe, F. Davidson, C. N. McEwen, *Eur. J. Inorg. Chem.* **2008**, *2008*, 2386.
- [29] F. Hennersdorf, J. J. Weigand, *Angew. Chem. Int. Ed.* **2017**, *56*, 7858.
- [30] a) H. Lei, J. C. Fettinger, P. P. Power, *Organometallics* **2010**, *29*, 5585; b) S. Wang, M. L. McCrea-Hendrick, C. M. Weinstein, C. A. Caputo, E. Hoppe, J. C. Fettinger, M. M. Olmstead, P. P. Power, *J. Am. Chem. Soc.* **2017**, *139*, 6586.
- [31] a) G. L. Dunn, J. K. Donohue, *Tetrahedron Lett.* **1968**, *9*, 3485; b) G. O. Schenck, R. Steinmetz, *Chem. Ber.* **1963**, *96*, 520.
- [32] a) M. Hofmann, C. Höhn, F. W. Heinemann, U. Zenneck, *Chem. Eur. J.* **2009**, *15*, 5998; b) R. Bartsch, P. B. Hitchcock, J. F. Nixon, *J. Chem. Soc., Chem. Commun.* **1989**, 1046. DOI: 10.1039/D6SC01229A
- [33] C. Schwarzmaier, A. Y. Timoshkin, G. Balázs, M. Scheer, *Angew. Chem. Int. Ed.* **2014**, *53*, 9077.
- [34] a) W. Huang, P. L. Diaconescu, *Chem. Commun.* **2012**, *48*, 2216; b) S. N. Konchenko, N. A. Pushkarevsky, M. T. Gamer, R. Köppe, H. Schnöckel, P. W. Roesky, *J. Am. Chem. Soc.* **2009**, *131*, 5740; c) M. Scheer, U. Becker, E. Matern, *Chem. Ber.* **1996**, *129*, 721; d) M. E. Barr, B. R. Adams, R. R. Weller, L. F. Dahl, *J. Am. Chem. Soc.* **1991**, *113*, 3052.
- [35] A. D. Phillips, S. Hino, P. P. Power, *J. Am. Chem. Soc.* **2003**, *125*, 7520.
- [36] J. R. Pinkes, A. R. Cutler, *Inorg. Chem.* **1994**, *33*, 759.



Data Availability Statement

View Article Online
DOI: 10.1039/D6SC01229A

The data supporting the findings of this work is available in the main text and the electronic supplementary information. Primary research data for this work will be made openly accessible on Radar4Chem (<https://radar4chem.radar-service.eu/radar/de/home>) under the DOI: 10.22000/7wa7f1kdq20s260j. The primary data can be accessed for reviewing purposes under the link:

<https://www.radar-service.eu/radar/en/dataset/7wa7f1kdq20s260j?token=kAkBYvZKfaULMrubpTSj>.

Crystallographic Information Files (CIFs) have been deposited at the Cambridge Crystallographic Data Center (CCDC) under the deposition numbers 2529860-2529874. These data are provided free of charge by the joint CCDC and Fachinformationszentrum Karlsruhe Access Structures service.

